Electronic Supplementary Material (ESI) for Nanoscale.

Supplementary Information

Gold Nanoparticle Capture in Protein Crystal Scaffolds

Ann E. Kowalski,[a] Thaddaus R. Huber,[a] Thomas W. Ni,[b] Luke F. Hartje,[c] Karina L. Appel,[a] Jarad W. Yost,[a] Christopher J. Ackerson,[b] and Christopher D. Snow [a,*]

Department of Chemical and Biological Engineering, Chemistry, and Biochemistry and Molecular Biology, Colorado State University, Fort Collins, CO, USA

Email: Christopher.Snow@colostate.edu

This PDF File includes:

Reagents:

The following chemicals were purchased from Sigma-Aldrich and used without further purification: Gold (III) chloride trihydrate ($HAuCl_4$, ≥49.0% Au basis), L-glutathione reduced (GSH, ≥98.0%). The following chemicals were purchased from TCI America and used without further purification: N^{ε}-carbobenzoxy-L-lysine (N^{ε}-Cbz-L-lysine, >98.0%). Other reagents were purchased from Alfa Aesar, Thermo Scientific, and Sigma-Aldrich and used without further purification. Lithium sulfate (Li_2SO_4, ≥98.5%). Trimethylamine N-oxide (TMAO, ≥98%). Hydroxylamine solution (50 wt. % in H_2O). A blend of 1.83M malonic acid, 0.25M sodium citrate, 0.12M succinic acid, 0.3M D-L malic acid, 0.4M acetic acid, 0.5M sodium formate, and 0.16M sodium tartrate was titrated to pH 7.5 using sodium hydroxide, and was used in crystallization and crosslinking. This is a modified blend of Tacsimate™ from Hampton Research and is referred to as mTacsimate™ throughout the paper. The modification removes ammonium from the solution, which contains primary amines that interfere with protein crystal crosslinking.

Protein crystal preparation:

Periplasmic protein (Genebank ID: cj0420, Protein Data Bank code: 2fgs) from *Campylobacter jejuni* was selected from a scan of the Protein Data Bank for proteins that crystallize with large pores (Fig. S1). It was expressed in pSB3 in *E. coli* BL21 (DE3) pLySs using a glucose/lactose induction system at 17 °C for 36 hours.[1] The cells were lysed by sonication and purified via immobilized metal affinity chromatography. Purified protein was buffer exchanged into 150 mM NaCl, 10 mM HEPES, and 10% glycerol at pH 7.5. A variant of CJ was cloned to insert a tobacco etch virus (TEV) protease cleavage site between the protein and an N-terminal hexahistidine tag. After initial purification and buffer exchange, this protein was incubated with TEV protease (1:100 OD_{280}) overnight at 4 °C. Following TEV cleavage, the protein was reverse purified by immobilized metal affinity chromatography to remove TEV and uncleaved protein.

The purified protein was characterized with SDS-Page (Fig. S7) and crystallized overnight by sitting drop vapor diffusion at 20 ˚C in 20% TMAO and 65-80% mTacsimate™ at pH 7.5. Crystals were 20-50 μm in height x 100-200 μm in diameter. Prior to crosslinking, crystals were washed with a 90% mTacsimate™, 10% glycerol mixture at pH 7.5 for 30 minutes. Crystals were then transferred to a mixture of 90% mTacsimate™ and 10% glycerol at pH 7.5, and crosslinked for 2 hours by the direct addition of 1% glyoxal and 25 mM borane dimethylamine complex (DMAB). The crosslinking reaction was quenched by transfer into a solution of 0.3 M hydroxyalamine and 25 mM DMAB in 0.1 M citric acid and 0.15 M NaCl at pH 5.0. After crosslinking and washing, crystals retained smooth, hexagonal morphology and clear color.

DNASU Plasmid ID:

CjCD00089155

CJ Sequence:

Protein Sequence

MKEYTLDKAHTDVGFKIKHLQISNVKGNFKDYSAVIDFDPASAEFKKLDVTIKIASVNTENQTRDNHLQQDDFFKAKKYPDMTFTMKK
YEKIDNEKGKMTGTLTIAGVSKDIVLDAEIGGVAKGKDGKEKIGFSLNGKIKRSDFKFATSTSTITLSDDINLNIEVKANEKEGGSHHHH
HH**

DNA Sequence

TTAAGAAGGAGATATACATATGAAAAAAGTTCTGCTGAGCAGCCTGGTTGCAGTTAGCCTGCTGAGTACCGGTCTGTTTGCAAAA
GAATATACCCTGGATAAAGCCCATACCGATGTTGGCTTTAAAATCAAACATCTGCAGATTAGCAATGTGAAAGGCAACTTTAAAG
ATTATAGCGCAGTGATCGATTTTGATCCGGCAAGTGCAGAATTCAAAAAACTGGATGTGACCATTAAAATCGCCAGCGTGAATAC
CGAAAATCAGACCCGTGATAATCATCTGCAGCAGGATGACTTCTTCAAAGCCAAAAAATACCCGGATATGACCTTTACCATGAAA
AAATACGAGAAAATCGATAACGAAAAAGGCAAAATGACCGGCACCCTGACCATTGCCGGTGTTAGCAAAGATATTGTTCTGGAT
GCAGAAATTGGTGGTGTTGCCAAAGGTAAAGATGGCAAAGAAAAAATTGGCTTTAGCCTGAACGGCAAAATCAAACGTAGCGAT
TTCAAATTTGCAACCAGCACCAGCACCattACCCTGAGTGATGACATTAATCTGAACATTGAAGTGAAAGCCAACGAGAAAGAAGG
TGGTAGTCATCACCACCACCATCACTAATAACTCGAGCACCACCACCACCACCACTGAGATCCGGCTG

CJΔH6 Sequence:

Protein Sequence

MHHHHHHENLYFQGKEYTLDKAHTDVGFKIKHLQISNVKGNFKDYSAVIDFDPASAEFKKLDVTIKIASVNTENQTRDNHLQQDDFFK
AKKYPDMTFTMKKYEKIDNEKGKMTGTLTIAGVSKDIVLDAEIGGVAKGKDGKEKIGFSLNGKIKRSDFKFATSTSTITLSDDINLNIEV
KANEKE**TADDY

DNA Sequence

TCCCCTCTAGAAATAATTTTGTTTAACTTTAAGAAGGAGATATACATATGCATCACCACCACCATCACGAAAATTTGTATTTCCAG
GGAAAAGAATATACCCTGGATAAAGCCCATACCGATGTTGGCTTTAAAATCAAACATCTGCAGATTAGCAATGTGAAAGGCAACT
TTAAAGATTATAGCGCAGTGATCGATTTTGATCCGGCAAGTGCAGAATTCAAAAAACTGGATGTGACCATTAAAATCGCCAGCGT
GAATACCGAAAATCAGACCCGTGATAATCATCTGCAGCAGGATGACTTCTTCAAAGCCAAAAAATACCCGGATATGACCTTTACC
ATGAAAAAATACGAGAAAATCGATAACGAAAAAGGCAAAATGACCGGCACCCTGACCATTGCCGGTGTTAGCAAAGATATTGTT
CTGGATGCAGAAATTGGTGGTGTTGCCAAAGGTAAAGATGGCAAAGAAAAAATTGGCTTTAGCCTGAACGGCAAAATCAAACGT
AGCGATTTCAAATTTGCAACCAGCACCAGCACCattACCCTGAGTGATGACATTAATCTGAACATTGAAGTGAAAGCCAACGAGAA
AGAATGATGAACCGCCGATGATTATTGAGATCCGGCTGCTAACAAAGCCCGAAAGGAAGCT

Figure S1. Protein sequences

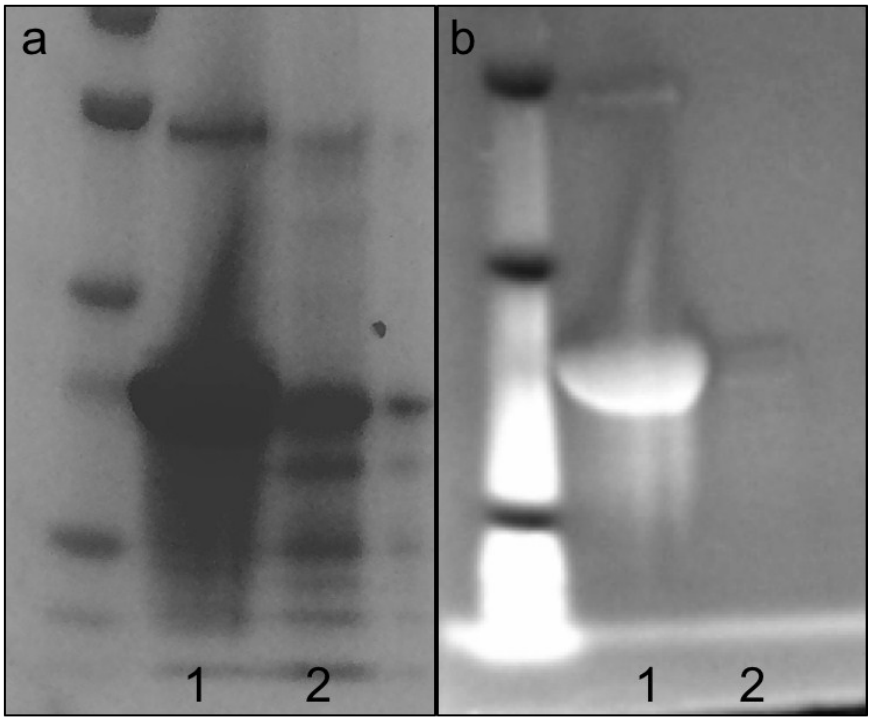

Figure S2. SDS-Page of purified protein samples (1) CJ and (2) CJ ΔH6 after (a) total protein staining by Coomassie and (b) InVision™ His-tag staining and UV transillumination.

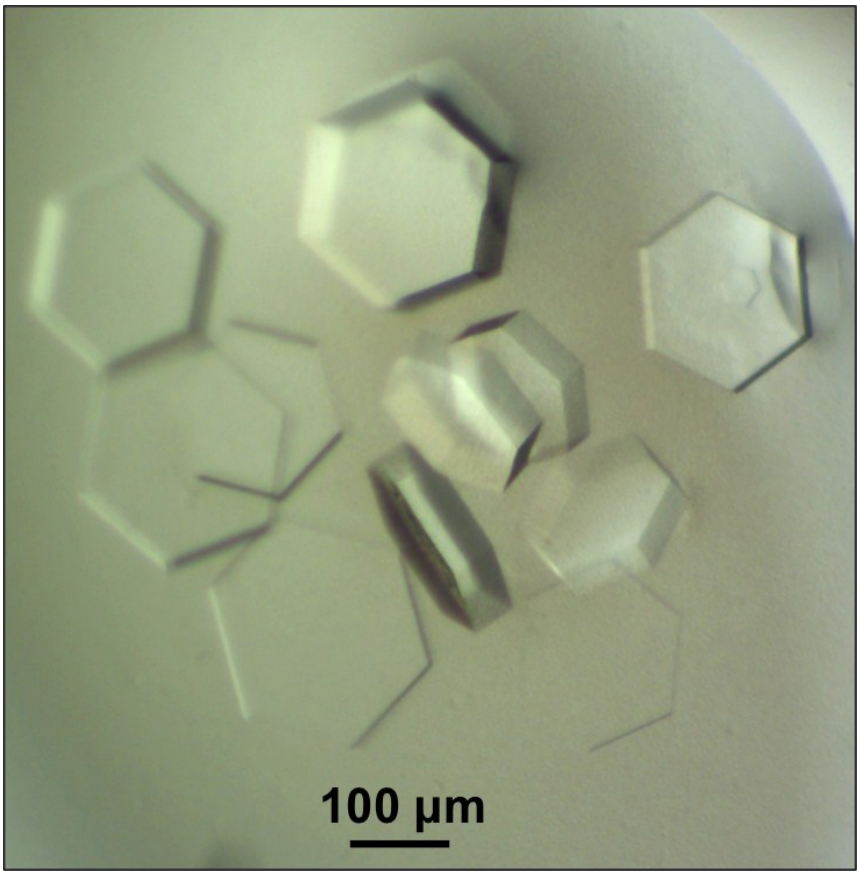

Figure S3. Representative growth well of CJ crystals in mTacsimate™

Gold nanoparticle synthesis:

$Au_{25}(GSH)_{18}$ was synthesized with a modified procedure briefly described here.[2] Glutathione (308.1 mg, $1x10^{-3}$ mol) was added to a solution of $HAuCl_4$ (98.7 mg, $2.5x10^{-4}$ mol) in 50 mL methanol. The solution was stirred to combine. The solution was initially a cloudy, yellow suspension, which after approximately five minutes of magnetic stirring turned to a clear and colorless solution. This solution was cooled at 0 °C while stirring for 30 minutes. To this, a solution of $NaBH_4$ (94.3 mg, $2.5x10^{-3}$ mol) in 12.5 mL ice H_2O was added rapidly with stirring. The reaction was allowed to stir for one hour at room temperature before the precipitate was spun down in 200 μL of 5 M NH_4OAc and MeOH at 4000 rpm. The supernatant was discarded and the precipitate was washed twice more in the same conditions and then dried. Gel purification was performed on $Au_{25}(GS)_{18}$ on a 24% polyacrylamide gel (Fig. S3).[3] $Au_{25}(GS)_{18}$ was extracted from the gel in H_2O and precipitated in MeOH and 200 μL of 5 M NH_4OAc and dried.

(1S)-N-(5-Carbobenzyloxyamino-1-carboxypentyl) iminodiacetic Acid (2). Ligand was synthesized using a previously published synthesis protocol.[4] Briefly, bromoacetic acid (4.17 g, 0.03 mol) was dissolved in 15 mL of 2 M NaOH. This solution was cooled to 0 ºC. To this a solution of N^{ε}-Cbz-L-lysine (4.2 g, 0.015 mol) in 22.5 mL of 2 M NaOH was added drop by drop and stirred for two hours at 0 °C. Stirring was continued overnight at room temperature. This solution was then heated to 50 °C for two hours, after which, 1 N HCl (45 mL) was added to the cooled solution. The precipitate was filtered and dried, to afford 1.5776 g of a crude white solid (**2, triacid**).

(1S)-N-(5-Amino-1-carboxypentyl)iminodiacetic Acid (3). A solution of **2** (6.8 g, 0.017 mol) in 95 mL MeOH/5 mL H_2O and a spatula tip full of 5% Pd/C catalyst was stirred with H_2 at 25 °C for 24 hours. Product was filtered through celite to remove the catalyst. The solvents were evaporated to give a colorless white paste.

(1S)-N-[5-[(4-Mercaptobutanoyl)amino]-1-carboxypentyl]iminodiacetic Acid (HS-NTA). The amino derivative (**3,** 1 g, 0.0038 mol) was dissolved in 10 mL H_2O with $NaHCO_3$ (1 g, 0.0119 mol) and 4-butyrothiolactone (0.6 g, 0.0059 mol) and stirred for 15 hours at 72 °C. The resultant mixture was acidified to pH 3 with acetic acid and concentrated under reduced

pressure. The crude product was crystallized in absolute ethanol, filtered and washed in absolute ethanol followed by pentane, and dried under vacuum to give a light beige solid (Scheme S1).

Ligand Exchange of $Au_{25}(GS)_{18}$. To dried and purified $Au_{25}(GS)_{18}$, five equivalents of HS-NTA was added and was dissolved in H_2O. The reaction was allowed to shake for 7.5 minutes.[5] The product was then precipitated out in methanol and 200 μL of 5 M NH_4OAc. Post centrifugation, the precipitate was dried under reduced pressure.

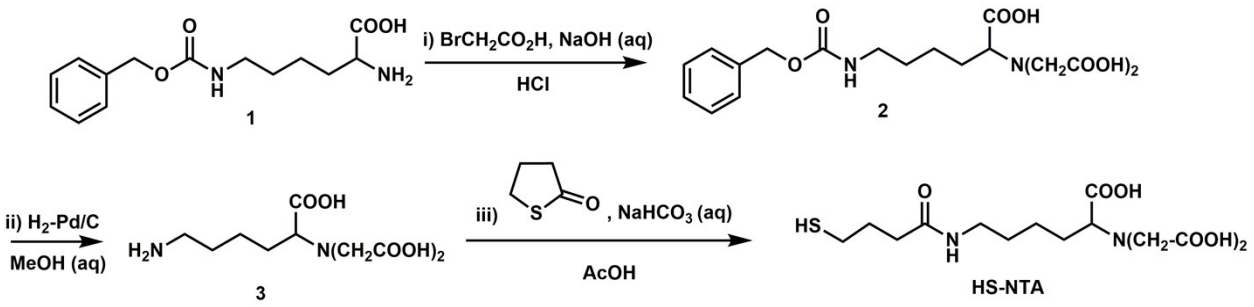

Scheme S1. Synthesis of HS-NTA.

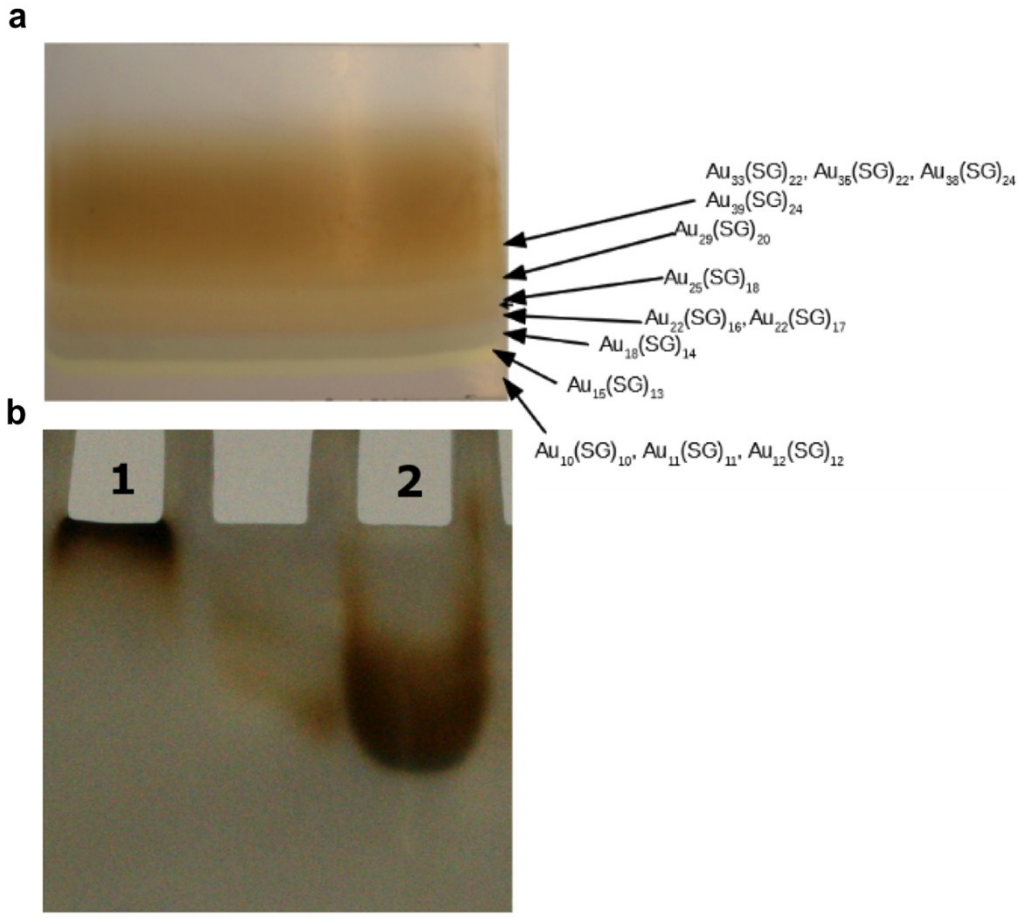

Figure S4. (a) Representative gel purification of crude $Au_{25}(GSH)_{18}$. (b) Representative gel of (1) $Au_{25}(GSH)_{18}$ and (2) $Au_{25}(GSH)_{17}NTA$. After ligand exchange the sample runs farther down the gel due to increased charge on the ligand layer.

Experimental Protocols:

Imaging. All nanoparticle uptake and release was carried out at room temperature with 10 µL samples of 1 mg/mL Au_{25} solution (with or without ligand exchange) in 50 mM MES at pH 5.0. Diffusion images were captured by exciting the particles with a low power 405 nm laser pointer and imaging the emission through a 450 nm longpass filter from Edmund Optics. Images of the $Au_{25}(GSH)_{17}(NTA)$ fluorescence standards and crystal z-stack in Fig. 3 were taken using an Olympus IX81 spinning-disk confocal microscope with Photometrics Cascade II camera, a 20×/0.5 numerical aperture objective with a 1x magnification changer, and Phasor holographic photoactivation system (Intelligent Imaging Innovations [3i], Denver, CO). Excitation was performed with a 561 nm diode laser and 692 ± 12.5 nm single bandpass emission filter to eliminate spectral crossover. Images were acquired and analyzed with SlideBook 6.0 software [3i]. To repudiate intrinsic crystal fluorescence, an empty crosslinked CJ crystal was imaged under the optical conditions used in Fig. 3 and found to exhibit average fluorescent intensity comparable to the 0 mg/mL $Au_{25}(GSH)_{17}(NTA)$ standard. For x-ray diffraction, crystals were protected in 50% mTacsimate™ and 22% TMAO at pH 7.5. A compact Homelab Rigaku with a microfocus X-ray generator and a Pilatus 200K detector was used at 60 second exposure and 93 mm detector distance.

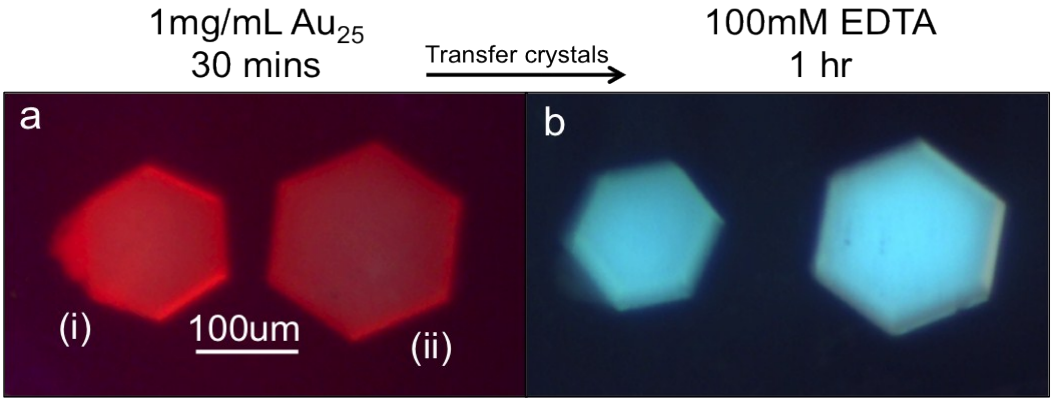

Figure S5. Each image contains a (i) CJ and (ii) CJΔH6 crystal. (a) At t = 30 mins in 1 mg/mL $Au_{25}(GSH)_{17}(NTA)$. (b) At t = 1 hr in 0.1M EDTA at pH 7.0. Imaged with 405 nm laser.

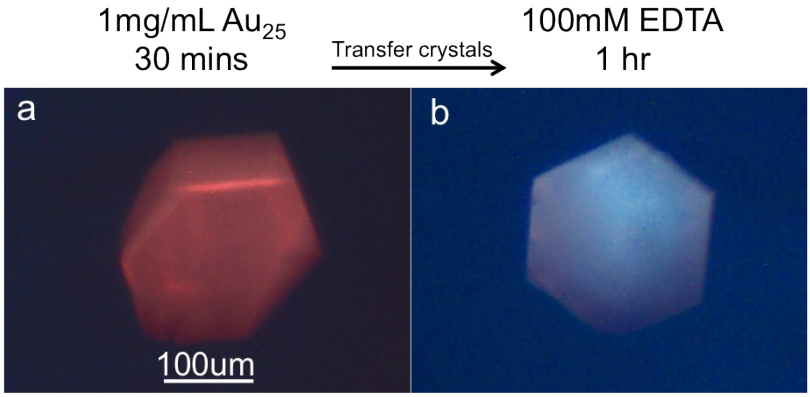

Figure S6. A CJ crystal after the fifth repetition of loading (a) At t = 30 mins in 1 mg/mL $Au_{25}(GSH)_{17}(NTA)$. and unloading (b) At t = 1hr in 0.1M EDTA at pH 7.0. Imaged with 405 nm laser.

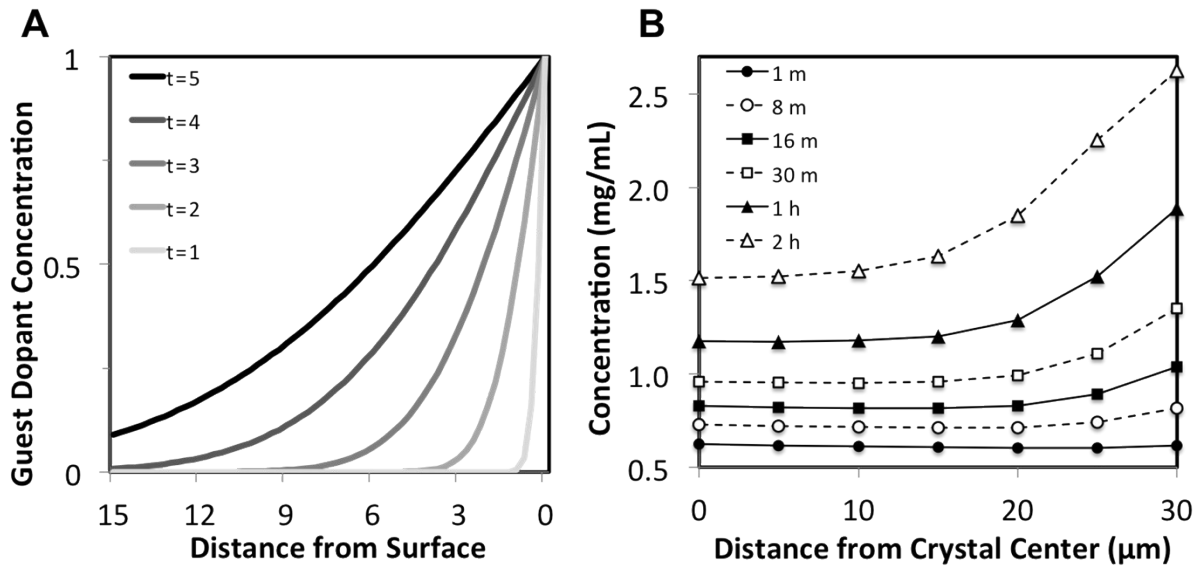

Figure S7. For simple diffusion (A), the concentration gradient just inside the host material decreases with time. This is illustrated here using a toy model for diffusion into a slab with D = 0.5 and fixed surface concentration Cs = 1. The concentration as a function of depth (x) and time (t) is governed by the following equation:

$$C(x,t) = C_s - (C_s - C_0)erf\left(\frac{x}{2\sqrt{Dt}}\right)$$

This model shows that under simple idealized diffusion in a plane sheet the concentration gradient just inside the host material decreases with time. (B) A CJ protein crystal was imaged by confocal laser microscopy while loading in 1 mg/mL $Au_{25}(GSH)_{17}(NTA)$ for 2 hrs. The gold nanoparticle concentration within the crystal was determined by comparing the fluorescence intensities of z-stack images to the fluorescence intensity standard curve used in Fig. 3. At 30 minutes, the concentration within the center of the crystal has reached that of the surrounding solution. However, the concentration gradient just inside the crystal continues to increase with time. This indicates strong adsorption within the crystal pores; standard boundary conditions (Dirichlet, Neumann, Robin) are inconsistent with the observed increases in surface concentration and increasing concentration gradient.

All images used in creating this graph were taken under identical optical settings and excited with a 561 nm diode laser.

X-ray Diffraction and Data Processing. CJ crystals were prepared using standard protocol and loaded with 1 mg/mL gold nanoparticles for 30 minutes. After loading, a similar crystal was unloaded in the presence of 0.1 M EDTA pH 7.0 for 30 minutes. Both crystals were briefly swished through a cryoprotectant solution containing 100% mTacsimate™ and 10% glycerol at pH 7.5 prior to flash freezing in a liquid nitrogen stream (T=100 K). Crystal integrity was determined via a 10 frame (0.5°/frame, 60 second exposure) data collection strategy on a local Rigaku Compact HomeLab with a micro-focus X-ray generator and a Pilatus 200K detector. Data was integrated and scaled using HKL3000 program suite and resolution estimated to 4.26 Å after loading in gold nanoparticles and 4.27 Å after unloading in EDTA.

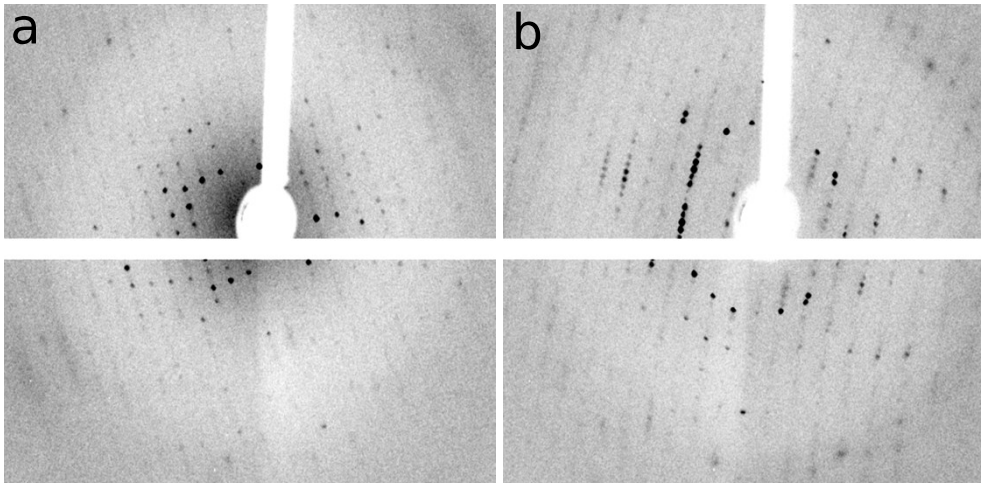

Figure S8. X-ray diffraction images of CJ crystal after incubation in (a) 1 mg/mL $Au_{25}(GSH)_{17}(NTA)$ for 30 min, followed by (b) 0.1 M EDTA at pH 7.0 for 30 min.

Lower Resolution (Å)	High Resolution (Å)	Average I	Average Error	CC1/2	CC*	
50	10.47	36.8	1.7	0.999	1	
10.47	8.33	12.6	1.2	0.989	0.997	
8.33	7.28	4.9	1	0.911	0.976	
7.28	6.61	5	1.1	0.995	0.999	
6.61	6.14	2.9	1.2	0.857	0.961	
6.14	5.78	4.1	1.3	0.816	0.948	
5.78	5.49	2.8	1.3	0.863	0.963	
5.49	5.25	3.1	1.4	0.786	0.938	
5.25	5.05	3.6	1.6	0.867	0.964	
5.05	4.88	3.4	1.6	0.671	0.896	
4.88	4.72	3.7	1.7	0.562	0.848	
4.72	4.59	3.9	1.8	0.866	0.963	
4.59	4.47	4.6	1.8	0.481	0.806	
4.47	4.36	5.7	1.9	0.061	0.338	
4.36	4.26	5.2	2.1	0.511	0.823	← High Resolution Estimate
4.26	4.17	2.6	2.1	0.25	0.633	
4.17	4.09	2.6	2.2	0.756	0.928	
4.09	4.01	2.2	2.2	0.424	0.772	
4.01	3.94	1.4	2.3	0.424	0.772	

Table S1. Scala output log for 10 frame diffraction check on a CJ crystal incubated in 1 mg/mL $Au_{25}(GSH)_{17}(NTA)$ for 30 min.

Lower Resolution (Å)	High Resolution (Å)	Average I	Average Error	CC1/2	CC*	
50	11.36	34.8	1.5	1	1	
11.36	9.03	21.7	1.2	0.988	0.997	
9.03	7.9	11.2	1	0.996	0.999	
7.9	7.18	7	1	0.984	0.996	
7.18	6.66	5.7	1.1	0.942	0.985	
6.66	6.27	4.7	1.1	0.733	0.92	
6.27	5.96	3.8	1.1	0.94	0.985	
5.96	5.7	4.4	1.2	0.915	0.978	
5.7	5.48	3	1.2	0.864	0.963	
5.48	5.29	3.3	1.4	0.922	0.979	
5.29	5.13	3.9	1.3	0.665	0.894	
5.13	4.98	5.1	1.5	0.851	0.959	
4.98	4.85	5.1	1.6	0.838	0.955	
4.85	4.73	6.5	1.5	0.962	0.99	
4.73	4.62	5.3	1.7	0.94	0.984	
4.62	4.52	6.9	1.7	0.752	0.927	
4.52	4.43	3.5	1.8	0.482	0.807	
4.43	4.35	4.7	1.7	0.541	0.838	
4.35	4.27	6.8	2.3	0.81	0.946	← High Resolution Estimate
4.27	4.2	6.5	2	0.342	0.714	

Table S2. Scala output log for 10 frame diffraction check on a CJ crystal after 30 min incubation in 1 mg/mL $Au_{25}(GSH)_{17}(NTA)$ min followed by 30 min incubation in 0.1M EDTA at pH 7.0.

To attempt to resolve a CJ gold nanoparticle co-structure, a more robust crosslinking method was performed. CJ crystals were grown at concentration of 10 mg/mL in 3.4 M $(NH_4)_2SO_4$, 0.1 M Bis-Tris at pH 7.0. Crystals were transferred to a well containing 3.2 M $(NH_4)_2SO_4$, 1 mM EDTA, 10% glycerol, 50 mM Bis-Tris at pH 6.5 and allowed to wash for 30 minutes. Crystals were then transferred to an amine free crosslinking solution containing 5 M TMAO, 0.5 M LiSO4, pH 7.5 (5T05L) and allowed to wash for 30 minutes. Crystals were crosslinked by transferring to 5T05L containing 1% glyoxal and incubating for 4 hours. Reductive stabilization of crosslinks was performed by a 30 minute incubation in 5T05L supplemented with 100 mM DMAB. After reduction, free aldehydes were quenched and reduced by addition of 50% hydroxylamine solution to 100 mM and incubating for 30 minutes. Crystals were loaded for 2 hours with gold nanoparticles under standard conditions. Visually, the resulting crystals appeared to have significant uptake of the gold nanoparticles (i.e. they turned red). Loaded crystals were swished through a cryoprotectant solution containing 5T05L prior to flash freezing in a liquid nitrogen stream. A full data collection set (360 frames, 0.5°/frame, 60 second exposure) was collected on the local Rigaku HomeLab. The data was reduced and integrated using iMosflm,[6] scaled using Pointless.[7] Molecular replacement was performed using Refmac[8] with 2FGS from the PDB as a starting model. X-ray diffraction data and refinement statistics are provided in Table S3.

Refinement of ambiguous electron density was kept conservative given the resolution. One strong, large, unmodeled electron density peak is between symmetry copies of Lys111 that could represent a glyoxal crosslinking product. It is difficult to model atoms here due to the 2-fold symmetry axis and the lack of chemical details about the crosslinking end product. The next largest unmodeled peak is, similarly, likely due to crosslinking at the interface that contains two Lys95 sidechains and two Lys98 sidechains. The next largest peak is the N-terminus, where fraying results in ambiguous electron density. Finally, a large peak is near the end of a possible ligand bound to the interior of the CJ barrel (CJ is a putative isoprenoid binding protein) that was here crudely modeled as an unsaturated alkane. Despite the 2 hr gold nanoparticle loading, after refinement there was no obvious peak corresponding to ordered gold nanoparticles in the porous structure of CJ.

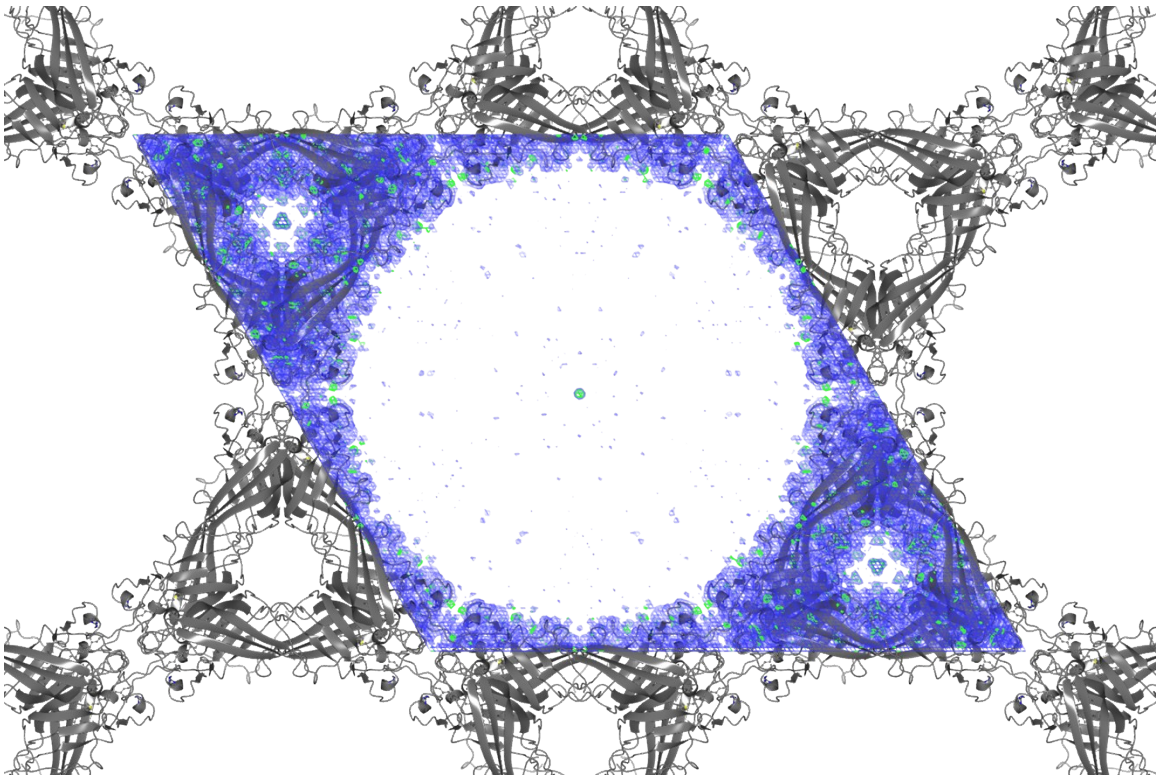

Figure S9. 2Fo-Fc map contoured to 1σ (blue) and Fo-Fc difference map contoured to 3σ (green) reveals no obvious preferred $Au_{25}(GSH)_{17}(NTA)$ binding sites in the crystal solvent pore after 2 hr incubation.

Data Collection		**CJ Au25 2 hr load**
Space group		P 6 2 2
Unit cell Dimensions:	a (Å)	178.461
	b (Å)	178.461
	c (Å)	50.1605
Total reflections		16044 (1244)
Unique reflections		8220 (750)
Multiplicity		2.0 (1.7)
Completeness (%)		0.99 (0.93)
Mean I/σ(I)		11.78 (1.10)
Wilson B-factor		56.65
R_{merge}		0.0621 (0.5722)
R_{meas}		0.08783 (0.8092)
$CC_{1/2}$		0.995 (0.59)
CC*		0.999 (0.862)
Refinement		
Reflections used in refinement		8207 (750)
Reflections used for R-free		398 (33)
R_{work}		0.2349 (0.3236)
R_{free}		0.2625 (0.3277)
CC(work)		0.943 (0.584)
CC(free)		0.886 (0.789)
RMS(bonds)		0.012
RMS(angles)		1.65
Average B-factor		55.12
macromolecules		55.47
ligands		48.46
solvent		30.58
Reflection statistics for the highest-resolution shell are shown in parentheses		

Table S3. X-ray diffraction data and refinement statistics for CJ crystal with 5T05L crosslink followed by 2 hour incubation in $Au_{25}(GSH)_{17}(NTA)$.

Elemental Analysis. The elemental analysis samples each consisted of three replicates, each containing three crystals loaded with gold nanoparticles and dissolved in 2 mL of aqua regia. Volumes were calculated by measuring side lengths and heights of the crystals. The first seven samples consisted of loading CJ crystals with $Au_{25}(GSH)_{17}(NTA)$ for the described length of time. For the eighth sample, CJ crystals were loaded with $Au_{25}(GSH)_{17}(NTA)$ for 30 minutes, then moved to a drop of 1 mM $NiSO_4$ in 20 mM HEPES pH 8.0. In the ninth sample, CJ crystals were loaded with $Au_{25}(GSH)_{17}(NTA)$ for 30 minutes, then moved to a drop of 0.1 M EDTA in 20 mM HEPES at pH 8.0. Elemental Analysis was performed at Midwest Laboratories, Inc.

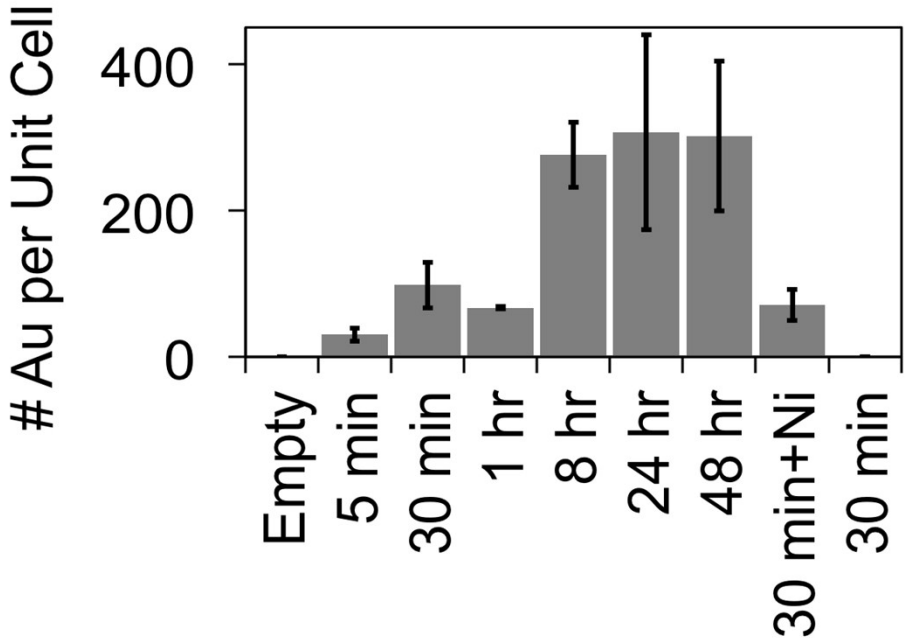

Figure S10. Number of Au atoms per unit cell of crystal as determined by elemental analysis. In the first seven samples, crystals were loaded with gold nanoparticles for 5 minutes to 48 hours. The eighth sample shows the gold nanoparticles retained by the crystal after loading for 30 minutes and releasing in the presence of Ni(II) for 1 hour. The final sample shows the full removal of gold nanoparticles after loading for 30 minutes and washing in the presence of EDTA for 1 hour.

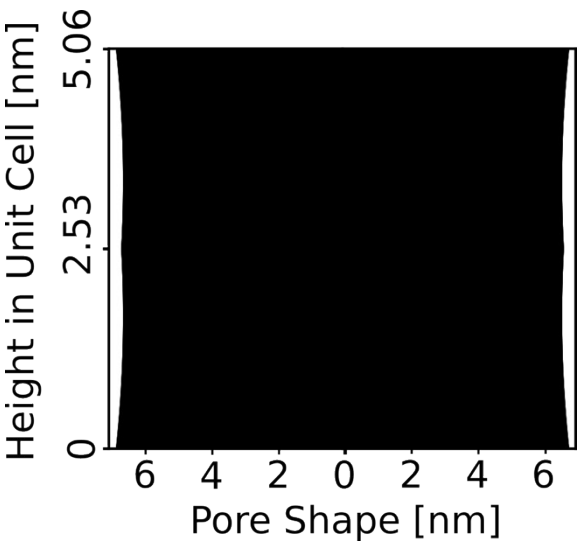

Figure S11. The pore diameter varies only slightly along the z-axis (13.1 to 13.6 nm). From any point along the pore center line, the minimum distance to a heavy atom in the protein crystal (including z-axis periodicity) is 6.57 nm.

References:

1. Studier, F. W. Protein production by auto-induction in high density shaking cultures. *Protein Expr. Purif.* **41,** 207–234 (2005).
2. Wu, Z., Chen, J. & Jin, R. One-Pot Synthesis of Au25(SG)18 2- and 4-nm Gold Nanoparticles and Comparison of Their Size-Dependent Properties. *Adv. Funct. Mater.* **21,** 177–183 (2011).
3. Negishi, Y., Nobusada, K. & Tsukuda, T. Glutathione-Protected Gold Clusters Revisited: Bridging the Gap between Gold(I)−Thiolate Complexes and Thiolate-Protected Gold Nanocrystals. *J. Am. Chem. Soc.* **127,** 5261–5270 (2005).
4. Sexton, J. Z. & Ackerson, C. J. Determination of Rigidity of Protein Bound Au(144) Clusters by Electron Cryomicroscopy. *J. Phys. Chem. C Nanomater. Interfaces* **114,** 16037–16042 (2010).
5. Heinecke, C. L. *et al.* Structural and Theoretical Basis for Ligand Exchange on Thiolate Monolayer Protected Gold Nanoclusters. *J. Am. Chem. Soc.* **134,** 13316–13322 (2012).
6. Leslie, A. G. W. & Powell, H. R. in *Evolving Methods for Macromolecular Crystallography* (eds. Read, R. J. & Sussman, J. L.) 41–51 (Springer Netherlands, 2007). at <http://link.springer.com/chapter/10.1007/978-1-4020-6316-9_4>
7. Evans, P. Scaling and assessment of data quality. *Acta Crystallographica Section D Biological Crystallography* **62,** 72–82 (2006).
8. Skubák, P., Murshudov, G. N. & Pannu, N. S. Direct incorporation of experimental phase information in model refinement. *Acta Crystallographica Section D Biological Crystallography* **60,** 2196–2201 (2004).

Appendix: Porous Crystal Volume Calculations

A1. Definitions

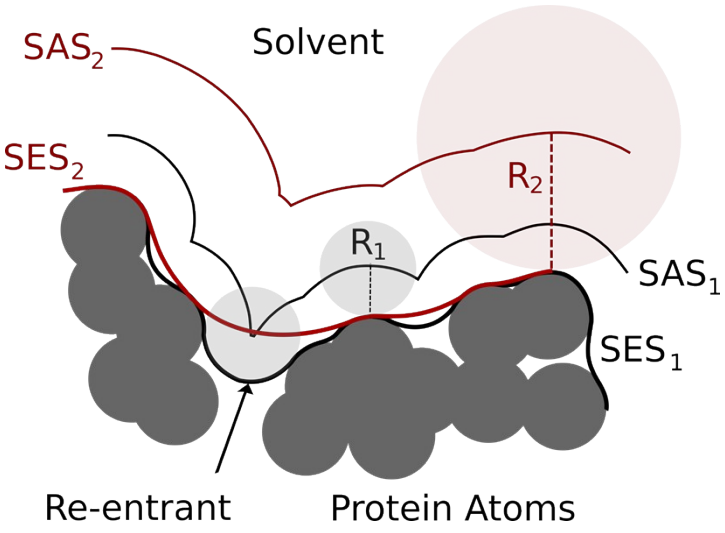

The term solvent excluded volume has been used to describe two different concepts. The first concept is to compute the volume that is inaccessible to the center of a probe sphere. This is the volume enclosed by the Lee & Richards solvent accessible surface (SAS)[1], so we term it sasV. The sasV value is relatively easy to compute. We just need to compute the volume for a union of spheres. Specifically, we place a sphere at each protein atom with the radius equal to the protein atom radius augmented by the probe sphere radius. This volume can be computed analytically using inclusion/exclusion (in exponential time), or more efficiently using algorithms that track which groups of protein atoms share volume. For example, Patrice Koehl, write code called **alphavol**[2], that efficiently computes the volume of the union of a collection of spheres.

The second concept is to compute the volume that is inaccessible to any portion of a probe sphere. This is the volume enclosed by the solvent excluded surface (SES), so we term it sesV. The sesV value is challenging to compute, since the SES surface (also known as the Connolly surface[3,4]) is comparatively challenging to compute exactly (i.e. rolling a sphere across the surface). The software **MSMS**[5] is commonly used to compute the area of the

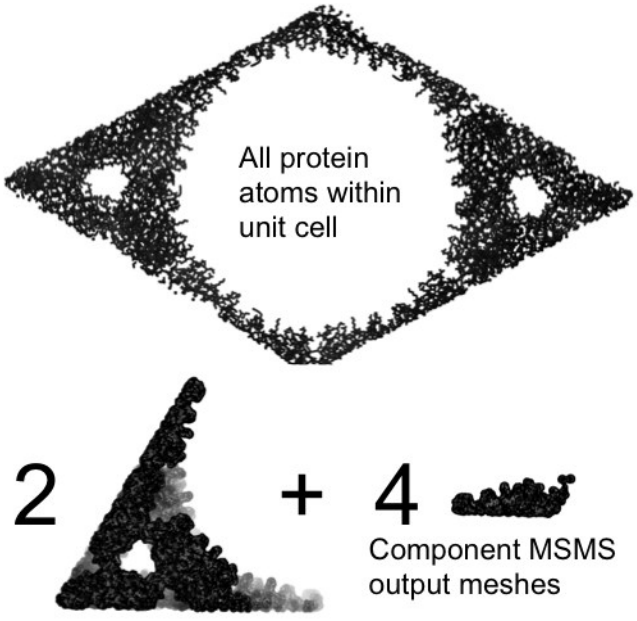

SES (i.e. the sesA). MSMS also reports a numerical sesV computation (the volume enclosed by the triangulated SES mesh).

A2. Crude Calculation

We can apply unit cell periodicity so that all atoms are present in one unit cell. The sesV of this collection of atoms provides a rough estimate for the sesV of the periodic unit cell. We can get a rough estimate of the solvent excluded volume (sesV) by running MSMS 2.6.1 on this model. This process is made more difficult since the model yields multiple disconnected components, and MSMS encounters a segmentation fault if asked to process all of these components (with the –all_components flag). However, the model can be broken into 2 large components each with ~118.5 nm^3 and 4 smaller components with ~8.5 nm^3 each. Thus, a rough estimate for the sesV of the unit cell is 271 nm^3. This number is approximate because MSMS was coded to handle freestanding monomers rather than periodic crystals.

A3. Calculating a Numerical Volume Given the SES Mesh

Fortunately, the triangulation output by MSMS facilitates the numerical calculation of the sesV. The triangles (ABC) that comprise the SES have a consistent ordering that allows the easy calculation of the volume of the polygon despite the many concavities. Given a reference point such as the origin, we can obtain the signed volume of the tetrahedrons formed by adding this reference point to each surface triangle[6,7].

$$V = \frac{1}{6}\left| \sum_{triangles,ABC} dot(\vec{A},\ cross(\vec{B},\vec{C})) \right|$$

A4. Precise Calculation via Mesh Truncation

Since we can directly calculate the volume enclosed by the SES mesh, we can improve our calculation of the sesV bounded by the unit cell by truncating the mesh at the unit cell boundaries. Briefly, our truncation algorithm **(1)** begins with a SES mesh calculated for one unit cell as well as protein atoms from neighboring unit cells within 10Å of the central unit cell, **(2)** identifies triangles in the mesh that cross a truncation plane at the unit cell boundaries, **(3)** truncates triangles that have two vertices out of bounds, **(4)** subdivides (into three smaller triangles) triangles with one vertex out of bounds, **(5)** connects new vertices placed on the

truncation plane into circular graphs that mark the perimeter of the intersection of the SES with the truncation plane, and **(6)** triangulates the area within this perimeter using a simple "ear clipping" algorithm. The cyan lines in the image below illustrate the triangulation of the six perimeters found when applying the last unit cell plane to truncate the mesh. With MSMS density set to 5.0, the corrected unit cell **sesV = 273.16 nm^3**.

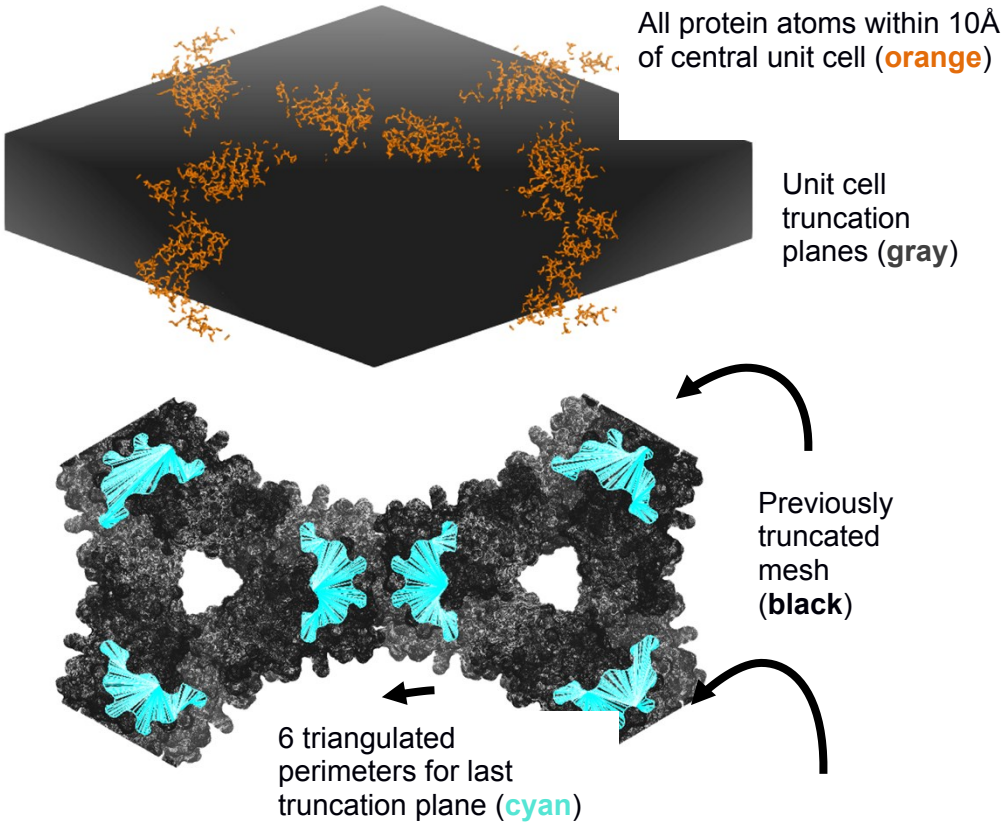

A5. Alternate Calculation via the Inclusion / Exclusion Principle

An alternate estimate is obtained using the inclusion/exclusion principle. In other words we can approximate the sesV for the 12 monomers in the unit cell using a multi-body expansion (accounting for 2-body and higher order corrections). We begin by running MSMS on an individual monomer. This gives 21,456 $Å^3$ excluded for each monomer (12 per unit cell). Next, we run MSMS on a domain swapped dimer. Each domain swapped dimer excludes 44402 $Å^3$, so the process of forming each dimer interface buries an additional 1,490 $Å^3$ (6 per unit cell). The other four smaller monomer-monomer interfaces bury an additional 1,152 $Å^3$ (6 per unit cell). These calculations were all done with a probe radius of 1.4 Å and MSMS density = 10.0.

In principle, where multiple proteins come together it is possible for there to be higher order corrections. For example, four monomers (the "tetramer" below) come close together where the orthogonal 2-fold axes intersect for the P622 spacegroup. However, candidate higher order terms were uniformly small (< $10Å^3$), and therefore neglected. Therefore, we estimate **sesV = 273.3 nm^3** solvent excluded volume per unit cell.

Model	Numerical		Analytical	
	sesV [Å^3]	sesA [Å^2]	sesA [Å^2]	sasA [Å^2]
monomer	21,456.0	10,250.2	10,287.2	12,747.6
domain swap dimer	44,402.3	16,907.4	16,984.0	18,887.6
dimer interface 2	43,458.3	19,819.5	19,885.1	24307.0
dimer interface 3	43,196.1	20,112.0	20,187.7	24,613.0
dimer interface 4	43,129.2	20,211.4	20,278.2	24,244.2
dimer interface 5	43,016.0	20,399.2	20,465.6	24,874.6
tetramer	89,422.8	32,818.5	32,959.4	34,756.6

Model	Numerical		Analytical	
	Δ sesV [Å^3]	Δ sesA [Å^2]	Δ sesA [Å^2]	Δ sasA [Å^2]
domain swap dimerization	1,490.4	-3593.0	-3590.4	-6607.6
interface 2 formation	546.3	-680.9	-689.3	-1,188.2
interface 3 formation	284.1	-388.4	-386.7	-882.2
interface 4 formation	217.3	-289.0	-296.2	-1250.9
interface 5 formation	104.1	-101.1	-108.8	-620.6
tetramerization	-7.4	-0.06	-0.02	-0.4

A6. Solvent Content Calculation

Given the results above, we can say that the static 2fgs model has a sesV of about 273 nm^3 per unit cell. Since the unit cell volume is 1411.8 nm^3, the sesV is only 19.4%. Equivalently, the 2fgs model of the crystal is 80.6% solvent. While different crystal structures might have (and be refined with) different unit cell dimensions, small variations do not greatly alter the solvent fraction. The unit cell volume is most sensitive to changes in the height, and a 1Å variation in the height keeps the solvent percentage at 80-81%.

A.7 Nanoparticle Accessible Volume Calculations

It would be useful to compute the volume from which nanoparticles are excluded. This provides a reference to interpret the apparent nanoparticle concentration in terms of packing density. Unfortunately, in our hands, MSMS experiences numerical issues with large probe radii. Additionally, nanoparticles such as $Au_{25}GSH_{18}$ are not perfectly spherical. Therefore, to estimate the volume within each unit cell that is available to be occupied by nanoparticles we have developed grid based (voxel) calculations.

Due to the size of the nanoparticles, there is a large difference between the nanoparticle sasV and the sesV. While about 33% of the crystal volume is accessible to the nanoparticle center of geometry, about 59% of the crystal volume is accessible to some portion of the nanoparticle. Briefly, the algorithm to compute these figures is: (1) Generating a model composed of all protein atoms within a unit cell (as above). (2) Generating an expanded version of this "stencil" that also includes protein atoms from neighboring unit cells if they are within 10 Å of the central unit cell. (3) Dividing this stencil into 18 angular wedges of 20° for faster subsequent collision checking. (4) Obtaining the nanoparticle coordinates (the same $Au_{25}GSH_{18}$ model mentioned previously), with the core gold atoms omitted for efficiency. (5) Efficiently scanning translations for the guest nanoparticle within the host crystal using a Fast Fourier Transform approach and grid representations of both the guest and the scaffold. (6) Explicitly checking the distance between border case candidate nanoparticle placements against the coordinates of 3 x 20° angular wedges of the scaffold (two flanking wedges of the home wedge for the nanoparticle placement). During this check, nanoparticle placements that are close to the protein scaffold (less

than 3Å between the van der Waal surface of a nanoparticle atom and a protein atom) are saved as possible models of adsorbed particles.

In the image below, each sphere represents a volume element of 0.84Å^3 distributed on a hexagonal grid array of 180 x 180 x 52. Voxel spheres are colored orange if they fall inside an "adsorbed" nanoparticle placement. While there were a few grid points in the minor axial pores that were far enough from the protein to pass the docking evaluation stage, only major axial pore placements were actually feasible upon explicit distance checks.

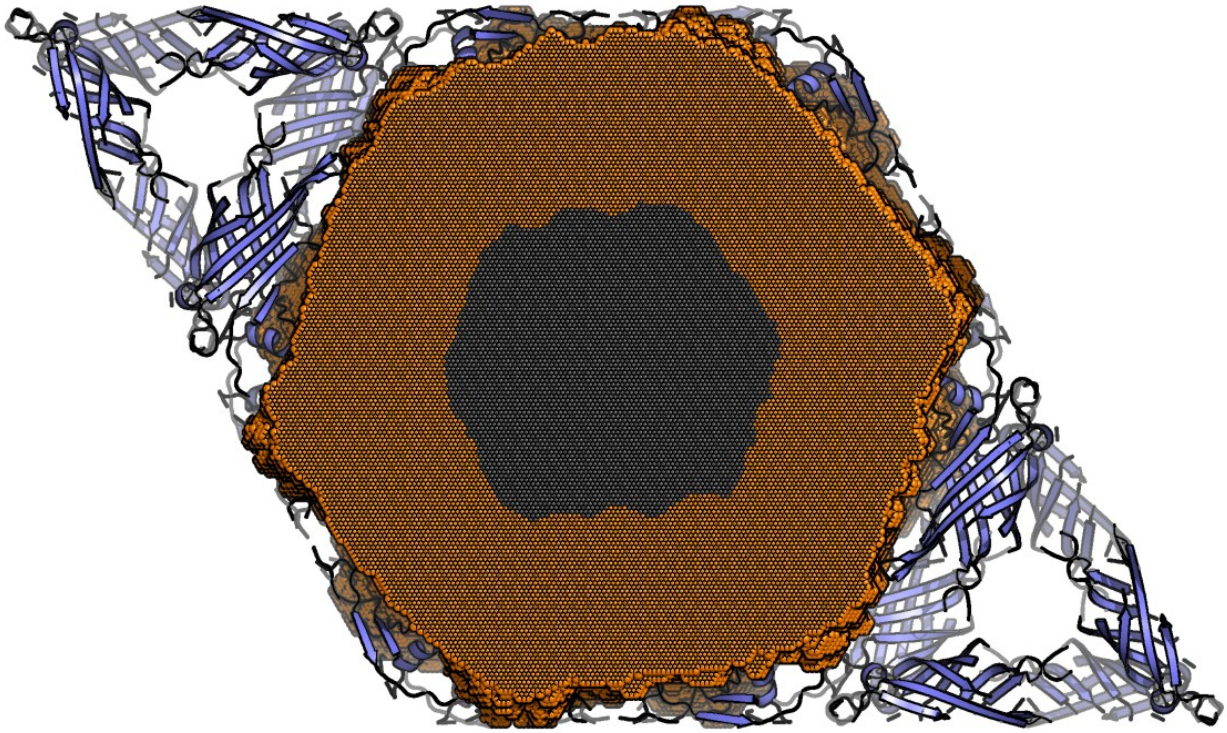

A.8 Adsorbed Nanoparticle Density

To provide physical intuition about the implications of the elemental analysis and confocal microscopy, we sought to investigate the maximum density with which nanoparticles might be placed inside the pores. A simple way to obtain a crude upper bound estimate would be to simply multiply the nanoparticle accessible volume in the crystals (833 nm^3 per unit cell, see above) by the maximum packing fraction of the nanoparticles in a crystalline form. However, the $Au_{25}GSH_{18}$ nanoparticles lack a crystal structure.

Instead, we can explicitly pack nanoparticles into the accessible volume. Since the goal of this exercise is simply physical intuition, we did not attempt to find a global optimum packing arrangement. Instead, we used a stochastic approach intended to mimic irreversible, "sticky" adsorption of the nanoparticles to the scaffold. In each of 25 random trials, prospective adsorbed nanoparticle placements (i.e. no more than a 3Å gap between the nanoparticle and the scaffold) were randomly shuffled. Then, candidate placements were considered iteratively, and accepted if they did not clash with previously accepted nanoparticle position (or with symmetry copies thereof). On the fine grid shown above, with a pool of 64,936 adsorbed nanoparticle positions, this nanoparticle packing algorithm yielded an average capacity of 17.5 nanoparticles adsorbed on the wall (standard deviation of 1.4). One high-density configuration with 21 nanoparticles is illustrated below.

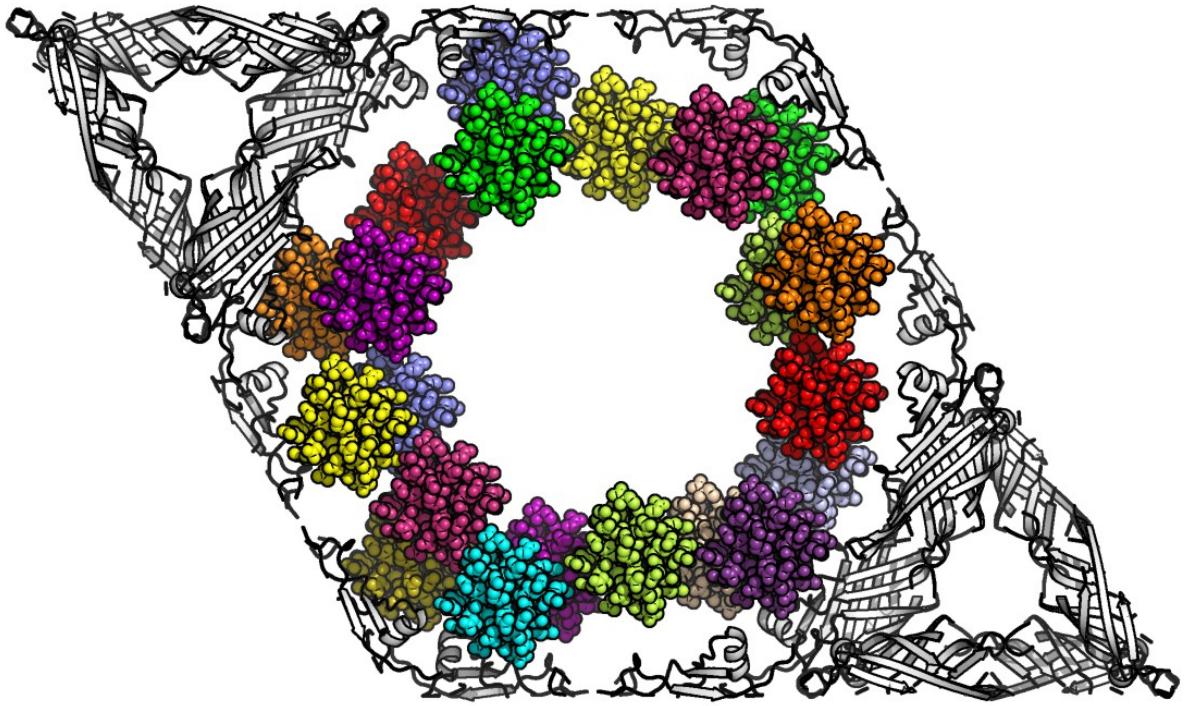

A9. Appendix References

1. Lee, B. & Richards, F. M. The interpretation of protein structures: Estimation of static accessibility. *Journal of Molecular Biology* **55,** 379–IN4 (1971).
2. Edelsbrunner, H. & Koehl, P. The weighted-volume derivative of a space-filling diagram. *PNAS* **100,** 2203–2208 (2003).
3. Connolly, M. L. Analytical molecular surface calculation. *Journal of Applied Crystallography* **16,** 548–558 (1983).
4. Connolly, M. L. Molecular surface Triangulation. *Journal of Applied Crystallography* **18,** 499–505 (1985).
5. Sanner, M. F., Olson, A. J. & Spehner, J. C. Reduced surface: an efficient way to compute molecular surfaces. *Biopolymers* **38,** 305–320 (1996).
6. Lien, S. & Kajiya, J. T. A symbolic method for calculating the integral properties of arbitrary nonconvex polyhedra. *IEEE Computer Graphics and Applications* **4,** 35–42 (1984).
7. Zhang, C. & Chen, T. Efficient feature extraction for 2D/3D objects in mesh representation. in *2001 International Conference on Image Processing, 2001. Proceedings* 3, 935–938 vol.3 (2001).